Mathematical Biology

Alain Goriely · György Károlyi · Michael Tabor

Growth induced curve dynamics for filamentary micro-organisms

Abstract. The growth of filamentary micro-organisms is described in terms of the geometry of evolving planar curves in which the dynamics is determined by an underlying growth process. Steadily propagating tip shapes in two and three dimensions are found that are consistent with experimentally observed growth sequences.

1. Introduction

The broad families of filamentary micro-organisms under investigation here are the prokaryotic actinomycetes and eukaryotic fungi. In the case of the actinomycetes, and the antibiotic producing streptomycetes in particular, the initial phase of cell growth consists of spores budding into long filamentary hyphae which grow in and on a nutrient medium (soil, in the case of many actinomycetes). As clearly demonstrated in experimental studies [8], growth in this phase is "apical", *i.e.* it occurs at the tip of the hyphae. The precise details of the growth mechanism, a complex process in which wall building polymers are incorporated into the tip as it is stretched by the intracellular fluid pressure (turgor pressure), are still not completely understood. As the tip is continually stretched and "rebuilt", the more remote portions of the hyphal wall rigidify, resulting in a steadily propagating finger-like structure that can grow to lengths of $50 - 100\mu m$ [7]. A typical time-lapsed hyphal growth sequence at a tip is shown in Fig. 1. It is usual for the growing hyphae to undergo a sequence of branchings - but here our concern is the modeling of a single hyphal tip. Filamentary fungi, which are typically much bigger than the actinomycetes [7], are also observed to undergo apical hyphal growth [9]. However, the internal cell structure and wall composition of the eukaryotic fungi is very different from the actinomycetes [7]. While turgor pressure is generally accepted to be the main driving force in the latter, its role in fungal growth is still a matter of discussion [10], [26]. Furthermore, the cytoskeleton is almost certainly involved in stretching

A. Goriely, G. Károlyi, M. Tabor: Program in Applied Mathematics and Department of Mathematics, University of Arizona, AZ 85721, USA.
e-mail: `goriely@math.arizona.edu`,
`www.math.arizona.edu/˜goriely; tabor@math.arizona.edu`

G. Károlyi: *Permanent address:* Center for Applied Mathematics and Computational Physics and Department of Structural Mechanics, Budapest University of Technology and Economics, Műegyetem rkp. 3., 1521 Budapest, Hungary
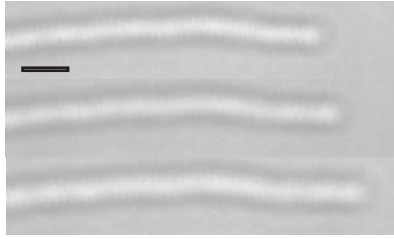
Fig. 1. Time lapsed sequence of hyphal growth of *Streptomyces coelicolor A3(2)*. Each image is 150 sec. apart. (bar is 1μm). Images collected courtesy Arizona Research Laboratories

the cell wall and transporting the wall building polymers, which are now contained in vesicles, to the tip [11,12].

Despite the very different underlying biology, the morphological similarities of hyphal growth in both families of organism has attracted the interest of researchers for some time, starting with the pioneering studies of streptomycetes by Reinhardt in the late 19th century [13]. Simplified growth models in which the filament is viewed as an elastic membrane under pressure have been discussed by Saunders and Trinci [15] and by Koch *et al.* [17], and recent work by the authors [18] has developed this approach into a biomechanical description of hyphal tip growth in terms of a three-dimensional bio-elastic membrane with geometry dependent moduli using large-deformation elasticity theory. A striking feature of this model is that it demonstrates, in keeping with the experimental observations, that the tip growth is of an essentially self-similar nature [19].

It is also possible to model apical growth according to "geometric", rather than biomechanical, principles. In such models (for earlier examples see [14], [9]) the increase in wall area of an advancing hyphal tip is balanced with the incorporation of wall building material - without specifying the details of underlying biological processes involved. This relatively simple, but intuitively appealing, approach can lead to the prediction of specific functional forms of the hyphal shape, such as in the work of Bartnicki-Garcia and co-workers [20,21] for fungal growth. The biological issues associated with their model have been discussed in the life-sciences literature [16].

These geometrical approaches can, in fact, be cast in the more general framework of the curve dynamics used to study the propagation of two-dimensional interfaces, such as seen in fluid dynamics and solidification [22], [3]; as well as in other areas of mathematical physics [4–6]. Here the interfaces are modeled geometrically as parameterized space curves, $\mathbf{X}(\sigma, t)$, whose kinematics is governed by dynamical rules reflecting the underlying physics [1,2]. The motion of such a curve is studied by decomposing its velocity into tangential $\mathbf{t}$ and normal $\mathbf{n}$ components, namely

$$\frac{\partial}{\partial t}\mathbf{X}(\sigma, t) = W\mathbf{t} + U\mathbf{n}, \tag{1}$$

where W, U denote, respectively, the tangential and normal velocities at each material point σ along the curve. These velocities are typically taken to be functions of

the curve geometry, namely its curvature, κ, and curvature derivatives, and plausible physical arguments can be used to determine specific forms of U and W. By considering the space curve as a representation of a (growing) cell wall this formalism is quite easily adapted to biological problems such as the morphogenesis of unicellular algae [23, 24] and, as will be described here, the modeling of hyphal growth. If the hyphae are considered to be axisymmetric, the (two-dimensional) contour represents a cross-section of the organism, but even then, as will be shown below, the three dimensionality of the growing structure can still be taken into account. It is interesting to note that although Reinhardt proposed over a hundred years ago that hyphal tip growth would only involve normal expansion, this has only been experimentally verified recently [27]. A consequence of this important result is that it is appropriate to set $W = 0$ in the velocity decomposition (1).

2. Basic equations of motion

The hyphal filament is modeled as an axisymmetric surface of revolution centered about the y-axis. This symmetry allows for a reduction to a plane curve lying in the (x, y)-plane pointing in the y-direction. Later we will exploit the axisymmetry to deduce three-dimensional filament shapes whose propagation is governed by rules for local areal growth. In keeping with experimental observations the filament, and hence the curve, is assumed to propagate with a steady velocity U_0 in the y-direction. The curve, parameterized in terms of arc length s, is taken to be of the form

$$\mathbf{X}(s, t) = (x(s, t), y(s, t) + U_0 t) \equiv (f(s, t), g(s, t) + U_0 t), \qquad (2)$$

with $s = s(\sigma, t)$ and where σ denotes a material coordinate. Of central importance in what follows is the metric variable

$$\lambda(s, t) = \frac{ds}{d\sigma}, \qquad (3)$$

which measures the stretching of material points along the curve. We will, in fact, assume that there is no explicit time dependence in f and g and hence write

$$\mathbf{X}(s(\sigma, t)) = (f(s(\sigma, t)), g(s(\sigma, t)) + U_0 t). \qquad (4)$$

The unit tangent and outward normal vectors are simply

$$\mathbf{t} = \frac{\partial \mathbf{X}}{\partial s} = (f_s, g_s), \quad \mathbf{n} = (-g_s, f_s). \qquad (5)$$

The curve can be reconstructed by integrating the differential equations

$$\frac{\partial x}{\partial s} = f_s = \cos\theta, \quad \frac{\partial y}{\partial s} = g_s = -\sin\theta, \qquad (6)$$

where θ is the "orientation" angle (see Fig. 2) and $\kappa = \theta_s$ the curvature.

There are various ways of expressing κ in terms of f and g; here we will use

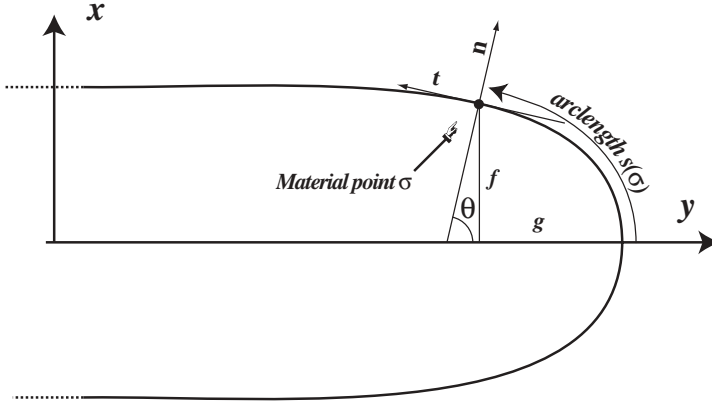$$\kappa = \frac{f_{ss}}{g_s} = \frac{-f_{ss}}{(1 - f_s^2)^{1/2}}. \qquad (7)$$

Fig. 2. Geometry of axisymmetric finger

In terms of the axisymmetric surface of revolution, κ corresponds to the longitudinal (or meridional) curvature. The other principal curvature (the latitudinal or azimuthal curvature) is given by

$$k = \frac{\sin\theta}{f}. \tag{8}$$

The velocity of the curve at any material point is

$$\frac{\partial \mathbf{X}(\sigma, t)}{\partial t} = (\dot{s} f_s, \dot{s} g_s + U_0), \tag{9}$$

where $(\dot{\,})$ denotes time derivative. The normal and tangential velocity components are thus

$$U = \mathbf{n}.\frac{\partial \mathbf{X}}{\partial t} = U_0 f, \quad W = \mathbf{t}.\frac{\partial \mathbf{X}}{\partial t} = \dot{s} + U_0 g_s. \tag{10}$$

We note that the normal velocity at a material point is the same as that of a fixed value of s; whereas the tangential velocity at a material point is the sum of the tangential velocity at a fixed value of s, namely $U_0 g_s$, and the rate at which s changes at that point. Equations (6) and (10) form a system of equations describing *all* kinematically possible shapes of the form (4). These three equations contain five unknowns, hence two of them must be set on biological ground or other assumptions. Based on observation [13,27] and simple energetics considerations, a basic assumption is that the points on the surface of the tip are moving normal to the surface and, accordingly, we set $W = 0$. Furthermore, in the following sections we relate the curvature of the curve or the surface to the growth rate of the surface: this is based on the fact that the curvature is maximum at the tip where growth is largest, and that no growth is observed along the straight wall segments [9,8]. The *normal growth* model $W = 0$ leads to

$$\dot{s} = -U_0 g_s. \tag{11}$$

Differentiating the left and right hand sides of (11) with respect to σ gives, respectively,

$$\frac{d\dot{s}}{d\sigma} = \frac{d}{d\sigma}\left(\frac{ds}{dt}\right) = \frac{d}{dt}\left(\frac{ds}{d\sigma}\right) \equiv \dot{\lambda}, \tag{12}$$

and

$$\frac{d}{d\sigma}(-U_0 g_s) = -U_0 \frac{dg_s}{d\sigma} = -U_0 \frac{ds}{d\sigma}\frac{dg_s}{ds} = -U_0 \lambda g_{ss}. \tag{13}$$

Thus we obtain

$$\frac{\dot{\lambda}}{\lambda} = -U_0 g_{ss}. \tag{14}$$

For the given choice of g_s it follows that

$$g_{ss} = -\theta_s \cos\theta = -\kappa f_s, \tag{15}$$

and hence that (14) is equivalent to

$$\frac{\dot{\lambda}}{\lambda} = U_0 \kappa f_s = \kappa U_0 \cos\theta \equiv \kappa U, \tag{16}$$

where $U = U_0 \cos\theta$ is the normal velocity at each point along the curve. This simple formula is, in fact, of value in analyzing experimental data since given a tip profile which is well enough resolved to enable computation of its curvature, and an estimate of U_0, it can be used directly to estimate the rate of wall stretching at each point along the tip.

3. Dynamics of line element and areal growth

The traditional approach to curve dynamics is to prescribe specific forms of the normal velocity U – usually as a function of κ and its derivatives. In this way a given choice of U determines the local stretching dynamics through (16). Here our approach is essentially the other way around. At the current level of modeling the propagation of hyphae is effectively determined by the rate at which material is incorporated into the hyphal tip. Accordingly, the modeling proceeds by prescribing plausible forms of the local areal growth rate and it is these choices that determine U and hence the tip shape $\mathbf{X}(s, t)$. Since the circumference of the tip at any point along the curve is simply $2\pi f$, a "band" of area around the (three dimensional) tip at that point is given by

$$\Delta A = 2\pi f \Delta s = 2\pi f \frac{ds}{d\sigma}\Delta\sigma = 2\pi f \lambda \Delta\sigma, \tag{17}$$

and hence

$$\frac{d}{dt}\Delta A = 2\pi\left(\dot{f}\lambda + f\dot{\lambda}\right)\Delta\sigma = 2\pi\lambda f\left(\dot{s}\frac{f_s}{f} + \frac{\dot{\lambda}}{\lambda}\right)\Delta\sigma. \tag{18}$$

Dividing both sides by ΔA gives

$$\frac{1}{\Delta A}\frac{d}{dt}\Delta A = \left(\dot{s}\frac{f_s}{f} + \frac{\dot{\lambda}}{\lambda}\right). \tag{19}$$

The left hand side of this equation, which denotes the growth of an area element per (unit) area element, has the dimensions T^{-1}. We interpret this as the rate at which new material is incorporated in the tip wall - a process that may depend on the location around the tip. We now make the ansatz

$$\frac{1}{\Delta A}\frac{d}{dt}\Delta A = N(s, t), \tag{20}$$

where $N(s, t)$ is some geometry dependent function that reflects the wall building process. It is convenient to write

$$N = N_0 n(s, t), \tag{21}$$

where N_0, which has dimensions T^{-1}, sets the fundamental time scale of the wall building process and $n(s, t)$ is a dimensionless function of tip geometry.

4. Two dimensional models

Given that the right hand side of (19) can be interpreted as the sum of (respectively) local latitudinal and longitudinal stretching rates, it may be of interest to consider a "two-dimensional" model in which only the longitudinal stretching rates are considered, *i.e.* the growth of a longitudinal line element. In this case the model reduces to

$$\frac{\dot{\lambda}}{\lambda} = N_0 n(s, t). \tag{22}$$

Equating (16) and (22) gives

$$\kappa U_0 f_s = N_0 n(s, t), \tag{23}$$

and hence

$$\frac{f_s f_{ss}}{\left(1 - f_s^2\right)^{1/2}} = -\alpha n(s, t), \tag{24}$$

or equivalently

$$\cos\theta\frac{d\theta}{ds} = \frac{1}{\alpha}n(s, t), \tag{25}$$

where $\alpha = N_0/U_0$, which has dimensions L^{-1}, identifies a natural length scale associated with the wall building process (albeit at the level of the curve dynamical model). An analogous length-scale was identified in the model of Bartnicki-Garcia *et al.* [20] and endowed with a special biological significance. Equation (24) can be written in the equivalent form which is the one used in the following computations.

Different tip shapes can now be determined by choosing different rate functions $n(s, t)$. Given the widely accepted "soft-spot" hypothesis of Reinhardt that growth is concentrated at the tip where the cell membrane is "softest", it is natural to make n proportional to tip curvature, namely $n(s, t) \propto \kappa^m$. This choice, with $m \geq 1$, ensures that growth is largest at the tip where curvature is largest, and tends to zero further along the hyphae [9, 8]. The linear choice $n \sim \kappa$ leads to the trivial solution $\theta =$ constant. Of more significance here is the quadratic relationship

$$n(s, t) = \frac{\kappa^2(s)}{\kappa_0^2},$$
(26)

where $1/\kappa_0$ is a characteristic length scale associated with the tip. The integration of Equation (25) then leads to the tip shape

$$y = \frac{1}{\alpha \kappa_0^2} \log(\cos(\alpha \kappa_0^2 x)),$$
(27)

which is shown in Fig 3. This particular form of tip shape, a reasonable match to observed hyphal tips, is not new – it has been given in the literature several times as an idealized form of a single dendrite used in studies of solidification [22]. If we set $\kappa_0 = \kappa(0)$, the curvature of the contour is
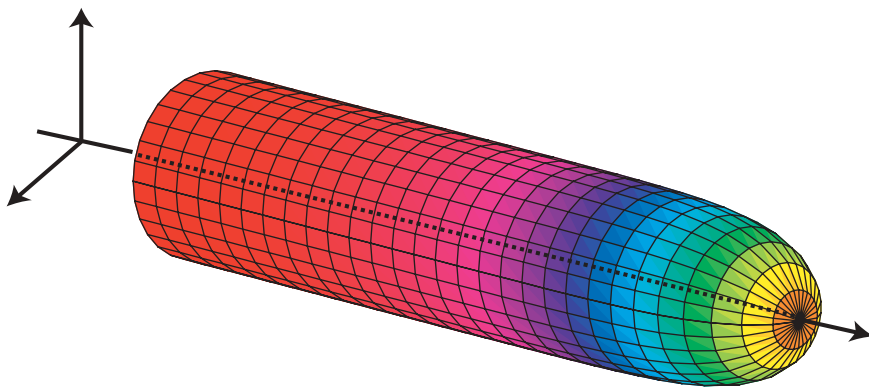
$$\kappa(s) = \frac{1}{\alpha} \text{sech}(s/\alpha),$$
(28)

so that the parameter $\alpha = \frac{1}{\kappa(0)}$ sets the tip curvature.

5. Three dimensional models

It is more realistic to analyze the tip growth from the point of view of rate of local areal growth. In this case we need to consider solutions to the equation

$$\left(\dot{s}\frac{f_s}{f} + \frac{\dot{\lambda}}{\lambda}\right) = N_0 n(s, t).$$
(29)

Fig. 3. Finger produced by line element growth proportional to the square of the curvature

Using (16) and $\dot{s} = -U_0 g_s = U_0 \sin\theta$, this can be written as

$$\cos\theta \left(\theta_s + \frac{\sin\theta}{f}\right) = \frac{1}{\alpha} n(s,t). \tag{30}$$

We note that the bracketed quantity on the left hand side is nothing more than the mean curvature of the axisymmetric shell. The presence of f in this equation renders it somewhat less tractable than before and one is essentially faced with having to solve the second order system

$$\theta_s = \frac{1}{\alpha} n(s,t) \sec\theta - \frac{\sin\theta}{f}, \tag{31}$$

$$f_s = \cos\theta, \tag{32}$$

with boundary conditions:

$$\lim_{s\to 0} (\theta, f) = (0,0), \tag{33}$$

$$\lim_{s\to\infty} (\theta, f) = (\pi/2, f_\infty), \tag{34}$$

where f_∞ is the asymptotic radius of the traveling finger. One now needs to consider appropriate choices for $n(s,t)$. Since we are considering the rate of local area growth, n should be chosen to reflect a property of the surface geometry and the wall mechanics. First, n must vanish on the side of a cylinder or on a flat surface. Second, n must be related to local properties of the surface and increase with local curvatures. Locally, the surface is characterized by its mean and Gaussian curvatures (K_m and K_g respectively). Since, the mean curvature does not vanish along cylinders, the dependence of n on the mean curvature is restricted to functions of the form $n(s,t) = K_g N(K_m, K_g)$ where $N(.,.)$ is analytic in its arguments and ultimately depends on the modeling of wall assembly. The simplest choice for N is to take it constant so that n is proportional to the Gaussian curvature which also appears naturally in the theory of thin plates (for instance in the theory of thin plates described by Föppl equations [31]). Therefore, we write

$$n(s,t) = \frac{K_g}{K_0} = \frac{1}{K_0} \kappa k = \frac{1}{K_0} \frac{\theta_s \sin\theta}{f}, \tag{35}$$

where K_0 represents a local area scale. This is the simplest possible relation between the surface growth and the curvature and we now explore the possibility of finger-like solutions. With this choice equations (31) and (32) reduce to the linear inhomogeneous equation
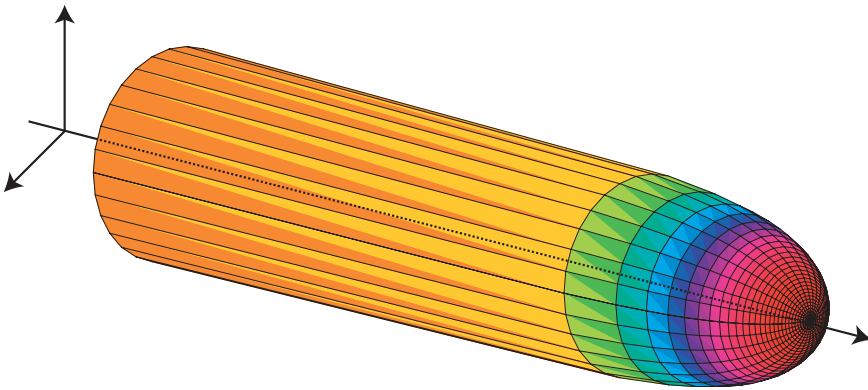
$$\sin\theta \frac{df}{d\theta} + \cos\theta f = \frac{1}{\alpha K_0} \sin\theta, \tag{36}$$

from which follows the exact solution

$$x(\theta) = \frac{1}{\alpha K_0} \left(\frac{\sin\theta}{\cos\theta + 1}\right), \tag{37}$$

$$y(\theta) = \frac{1}{\alpha K_0} \log\left(\frac{2\cos\theta}{\cos\theta + 1}\right). \tag{38}$$

Fig. 4. Finger produced by areal growth proportional to Gauss curvature ($\alpha = K_0 = 1$)

As shown in Fig. 4 this form has a nice-finger like structure. The associated principal curvatures are readily found to be

$$\kappa = \alpha K_0 \cos\theta (1 + \cos\theta), \tag{39}$$

$$k = \alpha K_0 (1 + \cos\theta), \tag{40}$$

and on setting $K_0 = K_g(0)$ it is easy to show that

$$K_0 = \frac{1}{4\alpha^2}. \tag{41}$$

Furthermore, using the standard trig identity $\sin\theta/(\cos\theta + 1) = \tan(\theta/2)$, it is possible to find the explicit extrinsic representation of the curve which takes the surprisingly simple form

$$y(x) = 4\alpha \log\left(1 - \frac{x^2}{16\alpha^2}\right). \tag{42}$$

A comparison of the 2-D and 3-D solutions is shown in Fig. 5.

6. Conclusion

In this paper the general kinematical feasibility conditions of growing, constant shape curves were formulated. These equations give the proper general description of tip-growth in filamentary microorganisms. However, to describe shapes for specific systems, further assumptions are required. Here we have shown that the assumption of normal velocity of material points observed in many systems together with a simple relation between curvature and surface growth may be reasonable representations of hyphal growth. This last assumption can easily be adapted to describe more complicated finger structures. It is important to stress that despite prior debates on the functional form of hyphal tips, this work shows that many different tip shape functions can be obtained based on reasonable curve-dynamical
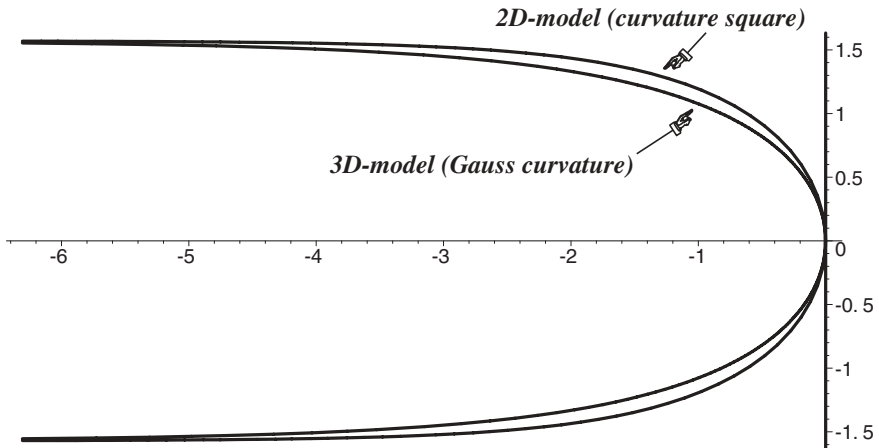
Fig. 5. The two profiles obtained with 2-D and 3-D growth (curvature square and Gaussian curvature)

assumptions. Although most of these shapes would make a reasonable fit to experimental data, little additional understanding of tip growth can be made solely based on such shapes without further knowledge of the actual biomechanical processes that generate them. Nonetheless, and in addition to the mathematical interest of this formulation, it still provides a tool for analyzing experimental data. Given a sequence of time lapsed images, such as shown in Fig. 1, it is possible to estimate the normal velocity of propagation U_0. Moreover, if a (reasonably high resolution) micrograph of the tip shape is available, it could fitted by one of the functional forms given here, such as (42). It would then be possible to estimate the length scale parameter α and hence, given the measurement of U_0, an estimate of the material deposition rate N_0. Even without an accurate fit to a specific functional form of the tip shape, a rate of longitudinal stretching could be estimated from (16). Overall, the main advantage of curve dynamical modelling is that it is a purely geometric approach that, within a few basic assumptions (such as the vanishing of tangential velocities), allows one to make exact statements on shapes, velocities and deposition rates. As such it is a valuable tool for analyzing data and building models for tip shapes. However, its main drawback is that it cannot reveal any information about the cell membrane stresses. Such information can only come from biomechanical models of hyphal growth such as those given in [18, 19].

References

1. Petrich, D.M., Goldstein, R.E.: A nonlocal contour dynamics model for chemical front motion. Phys. Rev. Lett. **72**, 1120–1123 (1994)

2. Uby, L.: Strings, rods, vortices and wave equations. Proc. Roy. Soc. London A **452**, 1531–1543 (1996)

3. Brower, R.C., Kessler, D.A., Koplik, J., Levine, H.: Geometrical models of interface evolution. Phys. Rev. A **29**, 1335–1342 (1984)

4. Langer, J., Perline, R.: Poisson geometry of the filament equation. J. Nonlinear Sci **1**, 71–93 (1991)

5. Goldstein, R.E., Petrich, D.M.: The Korteweg-de Vries hierarchy as dynamics of closed curves in the plane. Phys. Rev. Lett. **67**, 3203–3206 (1991)

6. Nakayama, K., Segur, H., Wadati, M.: Integrability and the motion of curves. Phys. Rev. Lett. **69**, 2603–2606 (1992)

7. Prosser, J.I., Tough, A.J.: Growth mechanisms and growth kinetics of filamentous micro-organisms. Critical Reviews in Biotechnology **10**, 253–274 (1991)

8. Gray, D.I., Gooday, G.W., Prosser, J.I.: Apical hyphal extension in *Streptomyces coelicolor* A3(2). J. Gen. Microbiol **136**, 1077 (1990)

9. Trinci, A.P.J., Saunders, P.T.: Tip growth of fungal hyphae. J. Gen. Microbiol. **103**, 243–248 (1977)

10. Money, N.P.: Wishful thinking of turgor revisited: The mechanics of fungal growth. Fungal Genetics and Biology **21**, 173–187 (1997)

11. Howard, R.J.: Ultrastructural analysis of hyphal tip cell growth in fungi: Spitzenkörper, cytoskeleton and endomembranes after freeze-substitution. J. Cell. Science **48**, 89–103 (1981)

12. Howard, R.J.: Cytoplasmic transport in hyphae of *Gilbertella*. Mycol. Soc. Am. Newsletter **34**, 24 (1983)

13. Reinhardt, M.O.: Das wachsthum der pilzhyphen. Jahrbücher für wissenschaftliche botanik **23**, 479–566 (1892)

14. da Riva Ricci, D., Kendrick, B.: Computer modelling of hyphal tip growth in fungi. Can. J. Bot **50**, 2455–2462 (1972)

15. Saunders, P.T., Trinci, A.P.J.: Determination of tip shape in fungal hyphae. J. Gener. Microbiol. **110**, 469–473 (1970)

16. Koch, A.L.: The problem of hyphal growth in streptomycetes and fungi. In: A.L. Koch (ed.), Bacterial Growth and Form, Chapman & Hall, New York, 1995, pp. 137–150

17. Koch, A.L., Higgins, M.L., Doyle, R.J.: Surface tension-like forces determine bacterial shapes: *Streptococcus faecium*. J. General Microbiol. **123**, 151–161 (1981)

18. Goriely, A., Tabor, M.: Self-similar tip growth in filamentary organisms. Phys. Rev. Lett. **90**, #108101 (2003)

19. Goriely, A., Tabor, M.: Biomechanical models of hyphal growth in actinomycetes. J. Theor. Biol. **222**, 211–218 (2003)

20. Bartnicki-Garcia, S., Hergert, F., Gierz, G.: Computer simulation of fungal morphogenesis and the mathematical basis for hyphal tip growth. Protoplasma **153**, 46–57 (1989)

21. Gierz, G., Bartnicki-Garcia, S.: A three dimensional model of fungal morphogenesis based on the vesicle supply center concept. J. Theor. Biol. **208**, 151–164 (2001)

22. Pelcé, P. (ed.): Perspective in Physics: Dynamics of curved fronts. Academic Press Inc., San Diego, 1988

23. Pelcé, P., Pocheau, A.: Geometrical approaches to the morphogenesis of unicellular algae. J. Theor. Biol. **156**, 197–214 (1992)

24. Pelcé, P., Sun, J.: Geometrical for the growth of unicellular algae. J. theor. Biol. **160**, 375–386 (1993)

25. Harold, F.M.: How hyphae grow: morphogenesis explained. Protoplasm **197**, 137–147 (1997)

26. Harold, F.M.: Force and compliance: rethinking morphogenesis in walled cells Fungal Genetics and Biology **37**, 271–282 (2002)

27. Bartnicki-Garcia, S., Bracker, C.E., Gierz, G., Lopez-Franco, R., Lu, H.: Mapping the growth of fungal hyphae: orthogonal cell wall expansion during tip growth and the role of turgor Biophysical Journal **79**, 2382–2390 (2000)
28. Grove, S.N., Bracker, C.E.: Protoplasmic organization of hyphal tips among fungi: Vesicles and Spitzenkörper. J. Bacteriology **104**, 989–1009 (1970)
29. Regalado, C.M., Sleeman, B.D., Ritz, K.: Aggregation and collapse of fungal wall vesicles in hyphal tips:a model for the origin of the Spitzenkörper. Phil. Tr. Royal Soc. London B **352**, 1963–1974 (1997)
30. Regalado, C.M., Sleeman, B.D.: Aggregation and collapse in a mechanical model of fungal tip growth. J. Math. Biol. **39**, 109–138 (1999)
31. Landau, L.D., Lifshitz, E.M.: Theory of Elasticity, 3rd Edition, Pergamon Press, Oxford, 1986